Characterization of Fuel Cell Electrode Processes by AC Impedance

Alternating current impedance measurements can be used as an *in situ* method for characterizing rate-limiting processes in fuel cell electrodes. Theoretical models have been derived and solved analytically. Theoretical analysis indicates that kinetic information can be extracted from the effect of temperature and gas composition on the size of the kinetic loop. The relative importance of kinetics and mass transfer can be inferred from AC impedance analysis. Several examples are given for the case of molten carbonate fuel cell (MCFC) electrodes. Such electrodes are not accessible to classical kinetic investigation techniques due to the high operating temperature and corrosive environment. Relevant kinetic information about MCFC electrodes has been obtained successfully using this *in situ* technique.

C. Y. Yuh, J. R. Selman
Department of Chemical Engineering
Illinois Institute of Technology
Chicago, IL 60616

Introduction

A fuel cell is an electrochemical device that can continuously transform the chemical energy of a fuel and an oxidant to electrical energy, by a process involving an essentially invariant electrode-electrolyte system. During the past decades, fuel cells have emerged as very efficient direct energy conversion devices. The molten carbonate fuel cell (MCFC) in particular, being an intermediate temperature device, looks promising (Selman and Marianowski, 1982).

The electrodes of a fuel cell are porous gas-diffusion electrodes. Such porous electrodes are usually under mixed control of electrode kinetics, mass transfer, and ionic conduction; therefore, the rate-limiting process cannot be described in simple terms. In the case of the MCFC cathode, no agreement exists in the literature about the detailed reaction mechanism and predominant reacting species (Yuh, 1985). This is due to the difficulty of access to an operating MCFC which, at 650°C or higher, is surrounded by insulation and forms a highly corrosive environment for any probe or intrusive measuring device. Yet, insight into the rate-limiting processes in the MCFC electrode is necessary to establish design criteria for the improvement of electrode performance. In a separate paper (Yuh and Selman, 1988), the rate-limiting processes in the MCFC anode and cathode are inferred from a large number of conventional stationary polarization data, which are interpreted by means of a semiquantitative analysis.

Correspondence concerning this paper should be addressed to J. R. Selman.
The present address of C. Y. Yuh is Energy Research Corporation Danbury, CT 06813.

In the present work, it is shown that alternating current impedance measurements also can be used to determine the rate-limiting processes at MCFC and other gas diffusion electrodes. AC impedance measurements are made *in situ* under various operating conditions. The analysis to be presented here demonstrates, as an example, that the results at open circuit are amenable to particularly simple methods of interpretation. Thus, AC impedance measurements are convenient tools for *in situ* determination of relevant process parameters.

In Situ Methods

In an AC impedance experiment, a small AC signal is used to perturb the electrochemical system and the response of the system is observed. At most frequencies, the AC signals in the time domain are measured over many cycles and then averaged; the impedance is then computed from the averaged voltage and current density signals, according to the defining equation $Z = \tilde{V}/\tilde{\imath}$. At very low frequencies, one cycle takes a long time and averaging is impractical; however, this is not a concern here because MCFC electrodes remain stable with respect to time over a time scale of months. Therefore, high-precision measurements are possible. Using small AC signals greatly simplifies the theoretical analysis because mass transfer and kinetic expressions can be linearized at the local polarization level.

Under these conditions, a planar electrode can be represented by an equivalent circuit (Bard and Faulkner, 1980). Similarly, in previous work a porous electrode has been represented by an appropriate equivalent circuit; this greatly simplifies the analysis.

The AC impedance method has been applied previously to relatively accessible porous electrodes, often in aqueous systems, whose structure and kinetics can be determined by other, *ex situ*, techniques. In this work, the AC impedance method is explored as an *in situ* diagnostic technique. *In situ* methods are especially attractive for the characterization of fuel cell electrodes for the following reasons:

1. Fuel cells are generally operated in compact configurations at elevated temperatures; therefore, the electrodes cannot be observed optically or probed in any convenient way. If the cell is cooled to ambient temperature and analyzed destructively, the structure and gas-liquid distribution results may not correspond to the original structure and distribution; changes occur because thermocapillary electrolyte movement takes place and thermal stresses fracture the electrode matrix. *In situ* electrochemical techniques are desirable which allow the characterization of the fuel cell electrodes without permanently altering performance-related characteristics.

2. An *in situ* method may allow one to extract kinetic or mass transfer parameters directly from measurements on an operating fuel cell electrode *in situ*. This is particularly important for the MCFC cathode, since the electrode kinetics and associated rate processes at a nickel oxide cathode are poorly understood and conflicting results, obtained under a variety of conditions in various types of cells, have been reported in the literature (Selman and Maru, 1983; Smith et al., 1982; Vogel et al., 1983; Winnick and Ross, 1981; Uchida et al., 1986). AC impedance measurements are a powerful alternative way of exploring the overall rate-limiting processes in the fuel cell itself under operating conditions.

Literature Review

Previous applications of AC impedance techniques to porous electrodes deal mostly with aqueous systems. The porous electrodes were usually flooded, that is, completely filled with liquid. Such electrodes are more typical of batteries than fuel cells. Nevertheless, their frequency response is of interest here since it reflects, in part, structural factors shared with gas-diffusion electrodes.

The AC frequency response of a cylindrical pore has been analyzed by de Levie (1967). His theoretical results have been confirmed experimentally. The effect of pore shape on AC impedance (in the absence of a charge transfer reaction) has been studied using a transmission line model (Keiser et al., 1976). The theoretical Nyquist diagram (real part vs. imaginary part of impedance) for a cylindrical pore was found to approach a 45° asymptote at high frequencies and a 90° asymptote at low frequencies. Experimental data were in good agreement with analysis.

Several other examples of AC impedance measurements at flooded electrodes are of interest because they have the objective of characterizing structure. A porous (sintered plate) cadmium electrode in alkaline solution was studied by Armstrong et al. (1975), who interpreted the results in terms of changes in wetted area and other factors.

The impedance of a gold-powder electrode and a Raney gold electrode (in the absence of a charge transfer reaction) were measured by Candy et al. (1981) and found to be very similar to those of a cylindrical pore of finite depth. The overall impedance of a packed-sphere electrode was also found to be similar to that of a cylindrical pore electrode. When the penetration depth approaches the pore depth, the shape of the pore wall has little influence on the impedance. For a Raney gold electrode Candy et al. found good agreement of their values of the structural parameters with those determined by other methods.

Candy et al. (1982) also determined the pore texture of a Raney nickel electrode. As expected, Raney nickel was found to have a double-scaled pore structure: one scale related to the micropores inside the catalyst grain, the other to a heaping of grains (macropores). The impedance measurement allowed *in situ* determination of the pore texture of a Raney nickel electrode filled with liquid.

The pore texture of a porous zinc electrode was characterized by Cachet and Wiart (1984). They found its AC impedance to be equivalent to those of a cylindrical pore electrode.

Delnick et al. (1983) determined the effective surface area of a Teflon-bonded carbon current collector by the impedance technique. Only a small fraction of the total internal surface area was found to be electrochemically active, that is, wetted.

In all instances discussed above, the charge transfer reaction was considered negligible. The impedance measurement was primarily aimed at the calculation of specific surface area and effective pore size. This was accomplished by means of simple network models. The primary interest of the present work, however, is to study charge transfer and mass transfer resistance and assess their importance relative to ohmic resistance in porous electrodes under mixed control. Therefore, an objective of the present work was to develop a model adequate for the interpretation of mixed-control behavior. Such a model is discussed next.

AC Impedance Model

Most porous-electrode models in the literature use a network of circuit elements. In the present work, however, a differential-equation model was developed to simulate the frequency response. Such a model has the advantage of simulating the behavior of activation and mass transfer polarization accurately.

A fuel cell porous-electrode model incorporating the effects of mass transfer, polarization level, and electrode microgeometry (macropore and micropore) has been developed specifically for application to MCFC electrodes (Yuh and Selman, 1984). It represents stationary polarization of such electrodes fairly well over a limited range of gas compositions and temperature (Yuh, 1985). Nevertheless, the complicated structure of any fuel cell electrode and the poorly known gas-liquid-solid distribution inside it make a complete and accurate simulation very difficult. Therefore, the AC impedance analysis presented here is that of a simplified model which assumes a high degree of uniformity in structure and local impedance. It will be shown that in spite of this simplification, the impedance of a MCFC porous electrode at open-circuit potential can be represented adequately by such a simple model.

An agglomerate model was developed for the analysis of the fuel cell porous electrodes. The development of this model starts with the agglomerate concept, which has been shown to represent fuel cell porous electrodes adequately for the analysis of stationary polarization (Giner and Hunter, 1969; Yuh and Sel-

man, 1984). The porous electrode consists of agglomerates of electrocatalyst particles (and of particles of carrier and other inert material, if present). The agglomerates contain the electrolyte completely within micropores formed by the interstices between their particles, and are themselves separated from each other by gas-filled channels (macropores). Two types of agglomerate structures are analyzed: cylindrical and planar, represented in Figure 1a.

Because ionic conduction takes place in the electrolyte, within the agglomerates, in a direction perpendicular to the plane of the porous electrode, Figure 1a, the agglomerates are considered continuous over the thickness of the electrode layer. The average cross section of the agglomerate is much smaller than the electrode thickness. Also, in a well-designed fuel cell electrode the gas-filled macropores are large enough to avoid significant gas phase diffusion resistance due to the electrode thickness. Under these conditions the main diffusion resistance is associated with transverse diffusion of dissolved gaseous reactants and products into the agglomerate, while the main ohmic resistance is axial, that is, in the thickness dimension of the porous electrode, Figure 1b.

Thus, concentrations are assumed to vary only in the transverse direction—perpendicular to the electrode thickness—while the potential of the electrolyte varies only in the axial (thickness) direction. This assumption has been used extensively in fuel cell electrode modeling (Giner and Hunter, 1969; Wilemski, 1983; Kunz et al., 1984; Yuh and Selman, 1984).

The models developed here are only valid at the open-circuit potential where the electrode is at equilibrium. In that case, average electrolyte potential and the concentrations of the various species are uniform throughout the electrode.

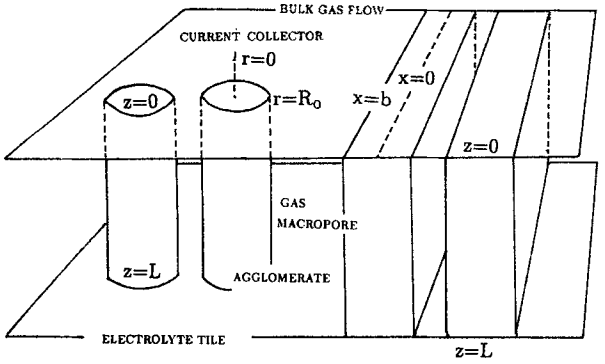

Figure 1a. Cylindrical and planar agglomerate structures.

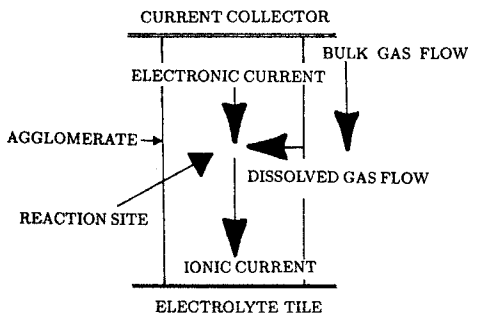

Figure 1b. Direction of current and reactant flow.

The following assumptions were made:

1. The electrode matrix and the electrolyte are homogeneously mixed as a continuum; the input parameters are porosity and specific surface area
2. The electronic conductivity of the electrode matrix is high enough to consider it isopotential
3. Ionic transport is represented adequately by Ohm's law
4. Electrolyte migration is considered unimportant due to the well-supported electrolyte system (concentrated phosphoric acid or molten carbonate in acid or molten salt fuel cells, respectively)
5. The intrinsic activity of the electrocatalyst is uniform throughout the electrode, as are all electrode-kinetic parameters
6. Linearized Butler-Volmer kinetics apply

The fuel cell reaction is generally expressed as:

$$\sum_i S_i R_i z_i \rightarrow ne^- \tag{1}$$

(See the Notation for definitions of all symbols.)

A mass balance for each reactant, C_i, in the agglomerate yields the following unsteady-state diffusion equations:

$$D_i \frac{\partial^2 C_i}{\partial x^2} - \frac{S_i a i_n}{nF} = \epsilon \frac{\partial C_i}{\partial t} \quad \text{planar} \tag{2}$$

$$\frac{D_i}{r}\frac{\partial}{\partial r}\left(r\frac{\partial C_i}{\partial r}\right) - \frac{S_i a i_n}{nF} = \epsilon \frac{\partial C_i}{\partial t} \quad \text{cylindrical} \tag{3}$$

A balance on the ionic current in the electrolyte yields the potential equations:

$$\bar{\kappa}\frac{\partial^2 \psi}{\partial z^2} + (a/b)\int_0^b i_n\,dx = -\left(\frac{aC_d}{b}\right)\frac{\partial}{\partial t}\int_0^b \eta_s\,dx \quad \text{planar} \tag{4}$$

$$\bar{\kappa}\frac{\partial^2 \psi}{\partial z^2} + \frac{2a}{R_o^2}\int_0^{R_o} i_n r\,dr = -\frac{2aC_d}{R_o^2}\frac{\partial}{\partial t}\int_0^{R_o}\eta_s r\,dr \quad \text{cylindrical} \tag{5}$$

As mentioned, concentrations are assumed to vary only in the radial (r or x) direction whereas potential varies only in the axial (z) direction.

To express the transfer current density, i_n, the Butler-Volmer kinetics are first linearized with respect to $\bar{\eta}_s$ and $\bar{C}_i$:

$$\begin{aligned} i_n \approx \bar{i}_n &+ i_o^b\left[\prod_i\left(\frac{\bar{C}_i}{C_{Ri}}\right)^{\gamma_i}\right] \\ &\cdot [\alpha_a\phi\exp(\alpha_a\phi\bar{\eta}_s) + \alpha_c\phi\exp(-\alpha_c\phi\bar{\eta}_s)](\eta_s - \bar{\eta}_s) \\ &+ i_o^b[\exp(\alpha_a\phi\bar{\eta}_s) - \exp(-\alpha_c\phi\bar{\eta}_s)]\sum_k \\ &\cdot\left\{\left[\gamma_k\left(\frac{\bar{C}_k}{C_{Rk}}\right)^{\gamma_k-1}\prod_{i\neq k}^{\pi}\left(\frac{\bar{C}_i}{C_{Ri}}\right)^{\gamma_i}\right](C_k - \bar{C}_k)\right\} \end{aligned} \tag{6}$$

at open circuit, $\bar{\eta}_s = 0$ and $\bar{i}_n = 0$. Therefore, Eq. 6 becomes:

$$i_n \approx i_o\phi(\alpha_a + \alpha_c)\eta_s \tag{7}$$

If only a small perturbation of current or voltage is applied to the porous electrode, the following approximations may be assumed:

$$i_n = \bar{i}_n + \tilde{i}_n = \bar{i}_n + \Delta i_n e^{j\omega t} \tag{8}$$

$$C_i = \bar{C}_i + \tilde{C}_i = \bar{C}_i + \Delta C_i e^{j\omega t} \tag{9}$$

$$\eta_s = \bar{\eta}_s + \tilde{\eta}_s = \bar{\eta}_s + \Delta \eta_s e^{j\omega t} \tag{10}$$

$$\psi = \bar{\psi} + \tilde{\psi} = \bar{\psi} + \Delta \psi e^{j\omega t} \tag{11}$$

Therefore, Eq. 7 becomes:

$$\Delta i_n = i_o \phi(\alpha_a + \alpha_c)\Delta \eta_s = A \Delta \eta_s \tag{12}$$

η_s and ψ are related according to:

$$\eta_s = -\psi + \frac{RT}{nF} \ln\left[\prod_i \left(\frac{C_i}{C_{Ri}}\right) S_i\right] \tag{13}$$

Equation 13 may be simplified to:

$$\eta_s = -\psi + \frac{1}{n\phi} \sum_i S_i \ln\left(\frac{\bar{C}_i}{C_{Ri}}\right) + \frac{1}{n\phi} \sum_i S_i \left(\frac{\tilde{C}_i}{\bar{C}_i}\right) \tag{14}$$

if $\tilde{C}_i \ll \bar{C}_i$.

Therefore:

$$\Delta \eta_s = -\Delta \psi + \frac{1}{n\phi} \sum_i S_i (\Delta C_i / \bar{C}_i) \tag{15}$$

By substituting Eqs. 8–12 and 15 into Eqs. 2 and 3, with subsequent nondimensionalization one obtains:

$$\frac{\partial^2 \Delta C'}{\partial \bar{x}^2} = \mathbf{M}_1 \Delta C' + \boldsymbol{M}_2 \Delta \Psi \quad \text{planar} \tag{16}$$

$$\frac{1}{\xi} \frac{\partial}{\partial \xi}\left(\xi \frac{\partial \Delta C'}{\partial \xi}\right) = \mathbf{M}_1' \Delta C' + \boldsymbol{M}_2' \Delta \Psi \quad \text{cylindrical} \tag{17}$$

The boundary conditions are

$$\bar{x} = 0, \quad \xi = 0 \quad \frac{\partial}{\partial \bar{x}} \Delta C' = 0$$

$$\frac{\partial}{\partial \xi} \Delta C' = 0 \tag{18}$$

$$\bar{x} = 1, \quad \xi = 1 \quad \Delta C' = 0 \tag{19}$$

Because $\mathbf{M}_1$, $\mathbf{M}_1'$, $\boldsymbol{M}_2$, and $\boldsymbol{M}_2'$ are matrices and vectors with constant coefficients and $\Delta\Psi$ is not a function of $\bar{x}$ or ξ, differential Eqs. 16 and 17 can be treated by the method of solving eigenvalue problems. If only one reactant, C_{R1}, is involved in the reaction, the solution is:

$$\Delta C_1' = [\alpha \cosh(\sqrt{M_1}\xi) + M_3]\Delta \Psi \quad \text{planar} \tag{20}$$

$$\Delta C_1' = [\alpha' \cosh(\sqrt{M_1'}\xi) + M_3']\Delta \Psi \quad \text{cylindrical} \tag{20}$$

Equations 4 and 5 are nondimensionalized. Substitution by Eqs. 8, 10, 11,12, and 15 yields:

$$\frac{\partial^2 \Delta \Psi}{\partial \zeta^2} = Q \Delta \Psi \quad \text{planar} \tag{22}$$

$$\frac{\partial^2 \Delta \Psi}{\partial \zeta^2} = Q' \Delta \Psi \quad \text{cylindrical} \tag{23}$$

with boundary conditions

$$\zeta = 0 \quad \frac{\partial \Delta \Psi}{\partial \zeta} = 0 \tag{24}$$

$$\zeta = 1 \quad \Delta \Psi = 1 - B \frac{\partial \Delta \Psi}{\partial \zeta} \tag{25}$$

Equations 22 and 23 can be solved analytically:

$$\Delta \Psi = \beta \cosh(\sqrt{Q}\zeta) \quad \text{planar} \tag{26}$$

$$\Delta \Psi = \beta' \cosh(\sqrt{Q'}\zeta) \quad \text{cylindrical} \tag{27}$$

The impedance is then, by definition:

$$Z = \frac{\Delta \psi_0}{(1 - \epsilon')\, \mathbf{A}\, \bar{\kappa} \left.\dfrac{\partial \Delta \psi}{\partial \zeta}\right|_{\zeta=1}} \tag{28}$$

Substituting Eqs. 26 and 27 into Eq. 28 yields:

$$Z = R_s + \frac{H \coth(\sqrt{Q})}{\sqrt{Q}} \quad \text{planar} \tag{29}$$

$$Z = R_s + \frac{H \coth(\sqrt{Q'})}{\sqrt{Q'}} \quad \text{cylindrical} \tag{30}$$

Now the assumption is made that mass transfer resistance is significantly smaller than other resistances (ohmic and kinetic). In that case,

$$C' \approx O \tag{31}$$

and the solutions of Eqs. 29 and 30 reduce to:

$$Z = \frac{H \coth(\sqrt{G})}{\sqrt{G}} \tag{32}$$

where $H = L/A\bar{\kappa}$ and G is a complex quantity given by: $(aL^2/\bar{\kappa})(A + j\omega C_d)$.

This solution is identical to that of a simplified AC impedance model (without Warburg impedance) developed by Yuh (1985). It is also similar to solutions derived by de Levie (1967) and Mund et al. (1982). Without charge transfer reaction, the Nyquist plot is the same as that predicted by de Levie and by Keiser et al. (1976): a 45° asymptote at high frequencies and a 90° asymptote at low frequencies, as shown in Figure 2a. The distance between the 90° asymptote and the imaginary axis is $R_s + (H/3)$. In the presence of a charge transfer reaction, Fig-

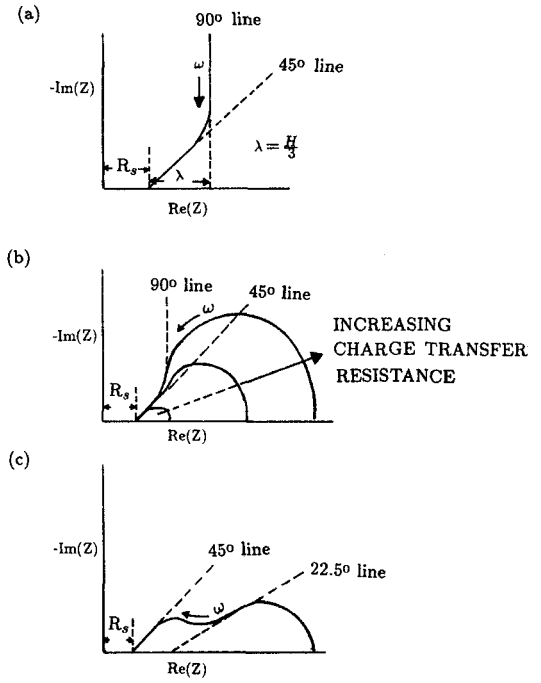

a. Ohmic conduction only
b. Ohmic conduction and charge transfer
c. Ohmic conduction, charge transfer, and mass transfer

Figure 2. Types of AC impedance response, simplified model.

ure 2b, the low-frequency part must come down to the real axis. Furthermore, the larger the charge transfer impedance, the smaller the angular frequency at the maximum in the Nyquist diagram. If mass transfer impedance is included, Figure 2c, a second loop at low frequencies occurs which takes off at a 22.5° slope. Thus, in spite of its simplicity this model is capable of a complete description of the frequency response of a porous electrode at its equilibrium potential. The values of the exchange current density may be estimated directly from the size of the kinetic loop.

In many systems, the parameter G is large; therefore, coth G is approximately equal to 1 and the total impedance, Z, becomes:

$$Z = \frac{H}{\sqrt{G}} \tag{33}$$

If the above approximation is valid, there are two ways of extracting kinetic information directly from an experimental Nyquist diagram; they are shown in Figure 3:

1. At very small frequencies, the kinetic impedance approaches ($R_s + a'$, 0), and the local kinetic impedance can be determined. The drawback is that the existence of mass transfer impedance at low frequencies (<0.5 Hz) makes the extrapolation uncertain.

2. At the maximum of the imaginary part, the total impedance Z is ($R_s + 3b'$, b'), and the corresponding angular frequency is $3A/C_d$. If the kinetic impedance is small, the angular frequency is large. Because the mass transfer impedance is usually appreciable only at low frequencies, the impedance at the maximum of the imaginary part may be assumed to be free of mass transfer resistance. Especially for a system with large

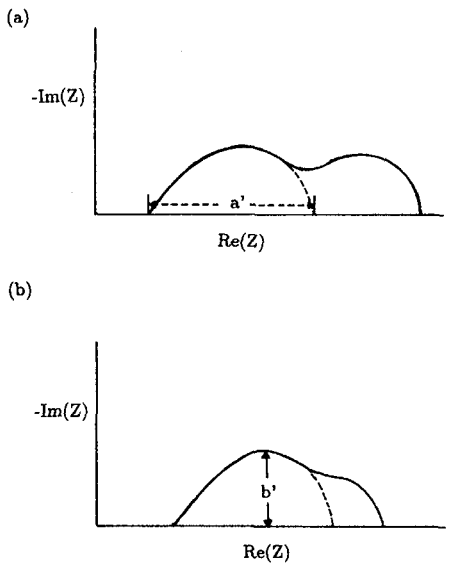

Figure 3. Two methods of determining the size of a kinetic impedance loop.

kinetic impedance, the mass transfer contribution is relatively small, though not always negligible, Figure 4. The height of the kinetic loop should be proportional to the square root of the local charge transfer impedance; thus, by comparing the heights for different gas compositions and temperatures, the reaction orders and activation energies can be determined.

Another method to extract kinetic impedance at low frequencies is to perform extrapolation or regression analysis of an impedance spectrum. A simple extrapolation technique has been developed for planar electrode systems such as the rotating-disk electrode (Smyrl, 1984). This is made possible by the simple analytical solution available for that case. A similar procedure was used by Uchida et al. (1986) to extract kinetic parameters for oxygen reduction in molten carbonate. For a porous electrode system, a simple analytical solution is in general not available; therefore, a nonlinear least-squares analysis is required based on the solution to Eq. 32 or 33. This type of analysis has been performed successfully by Yuh (1985) to determine i_o and C_d for a porous flow-through electrode system.

Determination of the charge transfer impedance at low frequencies by measuring the height of the high-frequency loop is

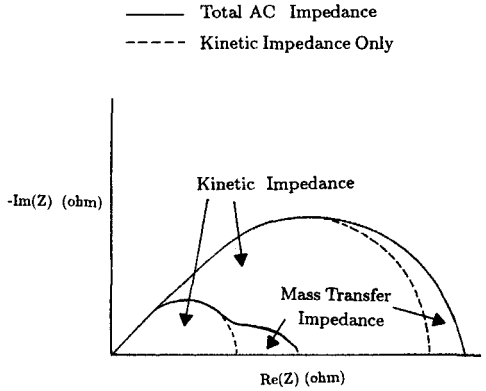

Figure 4. Effect of kinetic impedance on distribution of mass transfer impedance.

much easier and simpler than a regression analysis. Therefore, this technique is adopted here to study rate-limiting processes and reaction order in MCFC electrodes.

Equation 33 is valid only if G is large; in other words, the kinetic impedance does not approach that of a planar electrode at low frequencies, as shown in Figure 5. Therefore, experiments with inert gases must be carried out to ensure that the assumption ($G \gg 1$) is valid.

To determine the exchange current density, the total active surface area and effective ionic conductivity have to be known. The effective conductivity may be estimated from the rising portion of the Nyquist diagram (Yuh, 1985; Keiser et al., 1976).

Experimental Method

A state-of-the-art, laboratory-scale molten carbonate fuel cell (electrode area 3 cm^2) was used for the AC impedance measurements. The cell (Argano and Levitan, 1969) contained no metallic parts except for the electrodes and current collectors; the assembly is shown in Figure 6. The porous electrodes used in these experiments are Ni–10% Cr anode and nickel oxide cathode. A hot-pressed tile (62Li/38K carbonate in a porous $LiAlO_2$ support) was used as the electrolyte structure. The electrodes and electrolyte structure are stable for at least 5,000 h of MCFC operation, as demonstrated by various MCFC research groups (e.g., Institute of Gas Technology, Energy Research Corporation). The characteristics of the cell components are given in a separate publication (Yuh, 1988). The equipment used included a Wenking ST-72 potentiostat, a Solartron 1172 frequency response analyzer, and a Nicolet model 206 digital oscilloscope. The impedance measurements were carried out galvanostatically at about 15 different frequencies between 0.1 Hz and 2 kHz. It has been found that this frequency range is able to cover most of the Nyquist diagrams without introducing extraneous phase shift. On the Nyquist diagrams shown in this paper only data points at four typical frequencies (1, 10, 100, 500 Hz) were plotted. A small AC signal (<5 mA/cm^2 peak-to-peak) was used to perturb the system. A few other AC signal levels, as well as the potentiostatic mode, have also been used, with negligible difference. The Wenking potentiostat appeared to have a fast enough response time within the frequency range (<2 kHz). This was further confirmed by the AC impedance analysis of dummy cells, using the Wenking potentiostat. The cell was operated for a total of approximately 1,500 h. The performance

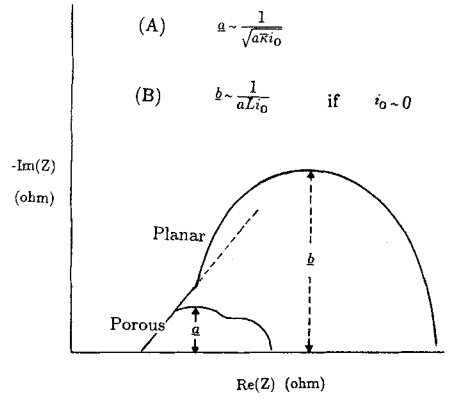

Figure 5. Effect of a, $\bar{\kappa}$, L, and i_o on frequency response of planar and porous electrodes, simplified model.

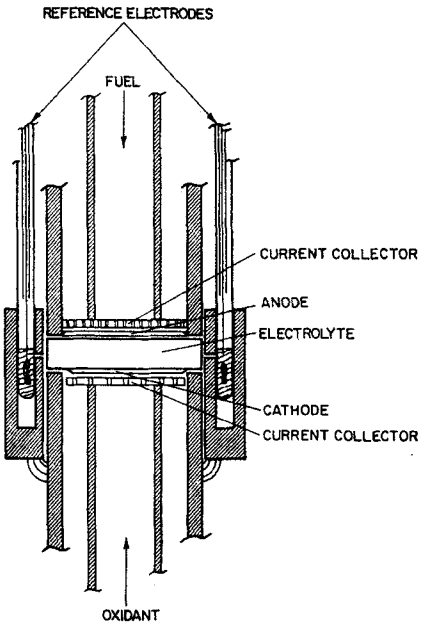

Figure 6. Laboratory-scale fuel cell assembly.

observed was standard and showed only a few mV decay during the course of an experiment. The electrochemical reactions, gas compositions and cell temperature were as shown in Table 1.

Results and Discussion

General characteristics

Most impedance results shown here were obtained at the equilibrium, open-circuit potential. Impedance results with superimposed DC polarization can be found in the thesis by Yuh (1985). An example with and without superimposed DC polarization is shown in Figure 7 for comparison. Little effect of the DC polarization on the general shape of the impedance diagrams is evident.

Figure 8 shows the Nyquist diagrams of anode and cathode with standard gases identified there. The high-frequency kinetic loops are easily identifiable and it is clear that the cathode impedance is much larger than that of the anode, mainly because of the slow cathode kinetics. Another important observation is the existence of a second (mass transfer) loop for the anode. The existence of a strong mass transfer resistance at the anode has long been suggested (Broers and Schenke, 1965) and the present data confirm this. This mass transfer polarization may be attributed to accumulation of reaction products (H_2O, CO_2) rather than to hydrogen depletion (Broers and Schenke, 1965).

Check on validity of the analysis

Before correlating the height of the kinetic loops with temperature or gas compositions, one must check if Eq. A in Figure 5 is valid for the experimental system. This was done using an inert gas; the results are shown in Figure 9. The cell potential was about 650 mV and can only be regarded as a quasi-equilibrium potential, since the theoretical equilibrium potential cannot be calculated mainly due to the unknown (very small) partial pressure of CO_2. The impedance results with inert gas should be affected by the cell temperature; however, this effect is quite

Table 1. Gas Compositions and Experimental Conditions

Anode reaction: $H_2 + CO_3^= \rightleftharpoons H_2O + CO_2 + 2e^-$
Cathode reaction: $\frac{1}{2}O_2 + CO_2 + 2e^- \rightleftharpoons CO_3^=$

Anode Gas Comp. (Dry), %			Cathode Gas Comp., %		
H_2	CO_2	N_2	O_2	CO_2	N_2
80	20	0	1.5	30	68.5
40	20	40	3	30	67
40	40	20	15	30	55
20	20	60	15	2	83
10	20	70	5	5	90
			5	5	90
			5	10	85
			10	5	85
			10	10	80
			10	60	30
			10	80	10
			10	90	0
			30	10	60
			50	10	40
			70	10	20
			90	10	0
			70	20	10
			70	30	0
			50	50	0
			33	67	0
			40	60	0

Cell temp.: 600, 650, 700°C; cell press.: 1 atm
Electrolyte: (62 mol % Li/38 mol % K)$_2CO_3$

small due to the weak dependence of the effective ohmic conductivity on temperature. It is clear that the Nyquist plot does not start rising or changing slope before approximately (0.4, −0.4). Examining the experimental data for normal oxidant, which are all at lower impedance values than (0.4, −0.4), one concludes that the assumption made in the interpretation of the kinetic loop according to Eq. A in Figure 5 is valid and that the height of the high-frequency loop is indeed the quantity a of Figure 5.

Fitting of high-frequency impedance spectra (i.e., charge transfer impedance) could be performed by carrying out nonlinear least-squares analysis using Eq. 32 or 33. A similar analysis has been attempted by Yuh (1985) for a flow-through electrode system to determine kinetic parameters. In the present paper, a simpler method is used to calculate i_o^b according to Figure 3. b' is found to be ~0.04Ω in 15% $O_2$30% $CO_2$55% N_2 gas at 650°C. Because $A = 3$ cm^2, $\alpha_a + \alpha_c = 3$ according to the superoxide mechanism, $\bar{\kappa} \approx 0.01\ \Omega^{-1}$ cm^{-1}, and $a \approx 5{,}000$ cm^{-1} based on the

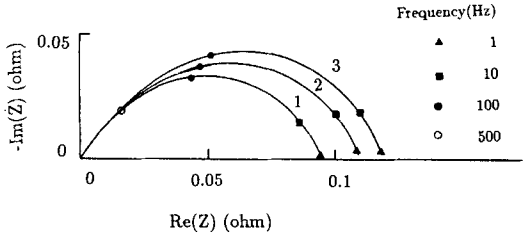

Figure 7. Cathode impedance data at 650°C with DC polarization.
Curve: *1*, 210 mA (anodic)
2, 0 mv (OCV)
3, 210 mA (cathodic)
Gas composition: 33% O_2/67% CO_2

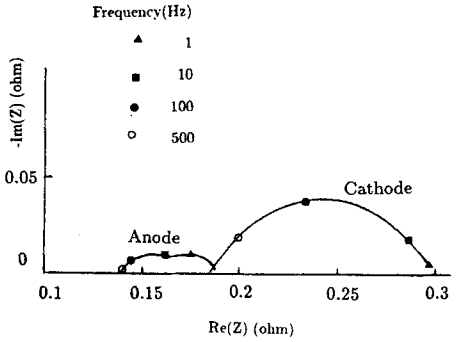

Figure 8. Anode and cathode frequency response with standard gas at equilibrium potential, 650°C.
Anode gas: 80% H_2/20% CO_2, humidified at 60°C
Cathode gas: 15% O_2/30% CO_2/55% N_2

available information on specific surface area of a NiO electrode, i_o^b is found to be ~5 mA/cm^2, which is the same order of magnitude as the results determined by Uchida et al. (1986).

Cathode impedance data

Most of the AC impedance results at equilibrium clearly show two distinct loops, except when the kinetic impedance is large. The effects of gas composition and cell temperature are shown in Figure 10–13.

The higher the P_{O_2}, the smaller the kinetic loop, Figure 10. This clearly indicates a positive reaction order for oxygen. For the data at higher P_{O_2} ($P_{O_2} > 0.7$ atm), where kinetics are likely to be rapid, a small mass transfer loop can be observed. For gas compositions having slower kinetics ($P_{O_2} < 0.15$ atm), the mass transfer loop cannot be distinguished, since it is masked by the large kinetic loop (that is illustrated in Figure 4). The maximum in the imaginary component of the high-frequency loop may include errors due to mass transfer; however, the errors are probably small, in view of the predominantly kinetic impedance.

For gases with 1.5 or 3% O_2, Figure 11, the kinetic resistance

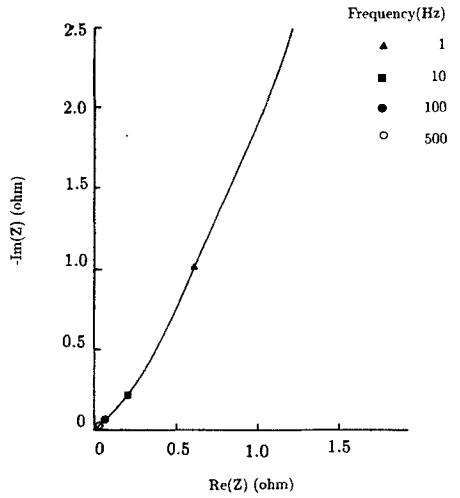

Figure 9. Cathode AC impedance with inert gas (30% CO_2/70% N_2) at quasi-equilibrium potential, 650°C.
Curve below 1 Hz represents actual data, not extrapolation

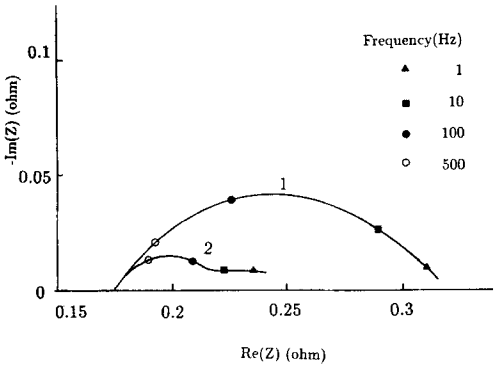

Figure 10. Effect of P_{O_2} on cathode AC impedance at equilibrium potential, 650°C.
Curve *1*: 10% O_2/10% CO_2/80% N_2
Curve *2*: 70% O_2/10% CO_2/20% N_2

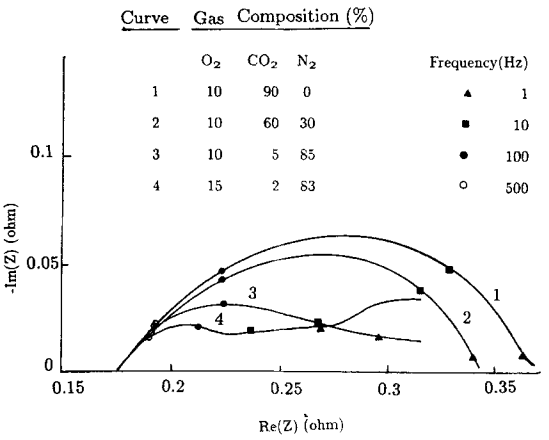

Figure 12. Effect of P_{CO_2} on cathode AC impedance at equilibrium potential, 650°C.

becomes so large that the mass transfer loops cannot be identified even though the mass transfer impedance is also expected to become large. It appears that the kinetic impedance increases at a faster rate than the mass transfer impedance as P_{O_2} is reduced.

According to Figure 12, the higher the P_{O_2}, the greater the kinetic resistance, implying that the reaction order of carbon dioxide must be negative. The mass transfer impedance therefore can easily be determined if P_{CO_2} is low (<0.1 atm) since the kinetics are then fast. The mass transfer impedance can be observed more easily in this case than when P_{O_2} is low. Both the kinetic and mass transfer impedances increase with decreasing P_{O_2}. This suggests that the mass transfer resistance limit is probably approached under normal operating conditions. On the other hand, a low P_{CO_2} yields a smaller kinetic impedance but a larger mass transfer impedance; hence, low P_{O_2} actually amplifies the mass transfer limitations. This phenomenon can be clearly observed in Figure 12, especially for the gas composition with 2% CO_2.

From Figure 13, it is evident that the cell temperature has a marked effect on AC impedance. In particular, the high-frequency loop is strongly affected by cell temperature. This is an independent confirmation that the first loop must be the kinetic loop, since the electrode kinetics normally have large activation energies. The low-frequency loop is only weakly affected by cell temperature; this loop therefore appears to be associated with the mass transfer, which normally has a much smaller activation energy.

Reaction orders of O_2 and CO_2

It has been shown that the maximum in the imaginary component of a kinetic impedance loop is approximately proportional to the square root of the local kinetic impedance. By correlating the maximum of the imaginary part with the gas compositions, the kinetic reaction orders can be inferred. Of course, this may be subject to minor errors, as discussed previously.

The empirical reaction orders of O_2 and CO_2 with the standard deviations obtained from a linear regression analysis at 650°C are shown in Table 2. The values of the reaction orders are closer to those of the superoxide mechanism (theoretical values 0.625 and −0.75, respectively) than to the peroxide mechanism (theoretical values 0.375 and −1.25, respectively). The above two mechanisms have been proposed by Appleby and Nicholson (1977, 1980a, b). The superoxide species was suggested by Smith et al. (1982) and Vogel et al. (1983) as the predominant species in Li/K melt.

Recently, Uchida and Nishina (1987) also concluded that the superoxide mechanism is predominant for the Li/K composition used in this study. The deviation from the theoretical parame-

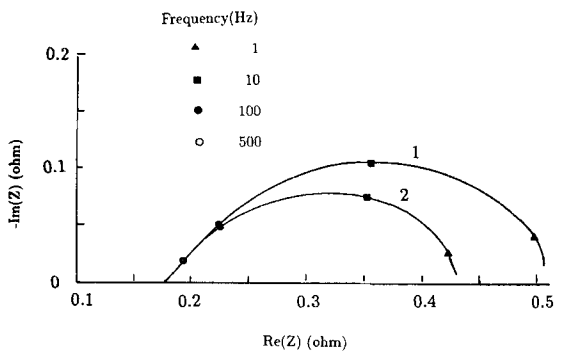

Figure 11. Effect of P_{O_2} on cathode AC impedance at equilibrium potential, 650°C.
Curve *1*: 1.5% O_2/30% CO_2/68.5% N_2
Curve *2*: 3% O_2/30% CO_2/67% N_2

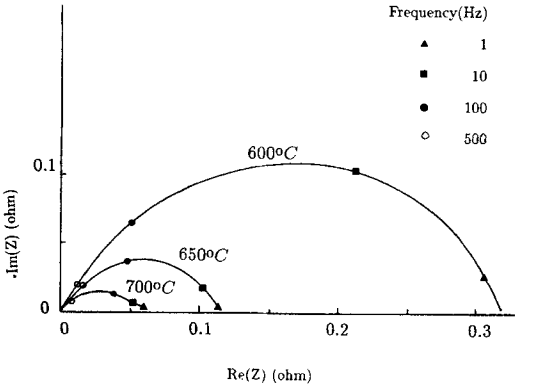

Figure 13. Effect of cell temperature on cathode AC impedance at equilibrium potential.
Gas composition: 15% O_2/30% CO_2/55% N_2

Table 2. Cathode Reaction Orders from AC Impedance

$i_o^o = i_o\,(O_2)^a(CO_2)^b$
Temp.: 650°C a 0.84 ± 0.02; b −0.45 ± 0.02

ters may be due to the effect of gas composition on the wetted surface area and on the effective conductivity. It is also possible that several electrochemical reactions occur simultaneously and that the electrochemical rate is not correlated adequately by a simple equation such as that in Table 2.

Conclusions

AC impedance characterization is a convenient and effective tool for investigating the relative importance of the various partial-rate processes in a gas-diffusion electrode with the help of theoretical models. The rate-limiting process can be identified from the effect of temperature and gas composition on the impedance components. If the experiments are carried out at the equilibrium potential, where the average concentration and potential are uniform, a relatively simple model is adequate for the theoretical analysis. The shape and size of the kinetic loop can then be represented by simple expressions containing the kinetic parameters. Kinetic reaction orders can thus be established as a step toward identifying the reaction mechanism. This is particularly important for the case of complicated multistep reactions under inaccessible cell conditions such as in a molten carbonate fuel cell.

Acknowledgment

This work was supported by the Electric Power Research Institute, Palo Alto, CA, under Contract No. RP-1085-2 and was carried out in part at the Institute of Gas Technology, Chicago, IL.

Notation

a = specific surface area of agglomerate, cm^{-1}
$A = i_o\phi(\alpha_a + \alpha_c)$
A = cross-sectional area of electrode, cm^2
$a' = 1(\sqrt{w}A)$
b = half-thickness of planar agglomerate, cm
$b' = 1/(\sqrt{8w}A)$
$B = [AR_s\bar{\kappa}(1-\epsilon')]/L$
C_i = concentration of species i, mol/cm^3
$C_i' = C_i/C_{Ri}$
$\bar{C}_i$ = average contration of species i, mol/cm^3
C_{Ri} = reference contration of species i, mol/cm^3
C_d = double layer capacitance, $Farad/cm^2$
D_i = effective diffusivity of species i, cm^2/s
F = Faraday constant
$G = (aL^2/\bar{\kappa})\,(A + j\omega C_d)$
$G' = aL^2A/\bar{\kappa}$
$H = L/A\bar{\kappa}$
i_o = exchange current density, mA/cm^2
i_o^b = bulk exchange current density under reference condition, mA/cm^2
i_o^o = standard exchange current density, mA/cm^2
i_n = transfer current density, mA/cm^2
I = Bessel function or current
Im = imaginary part of impedance
$j = \sqrt{-1}$
L = thickness of porous electrode, cm
$\mathbf{M}_1 = [A_{ij}]\,i = j,\ A_{ii} = (C_{Ri}\epsilon j\omega + aS_i^2A/n^2F\phi)(b^2/D_iC_{Ri})$
$i \neq j,\ A_{ij} = (S_iS_jAb^2C_{Rj}/n^2F\bar{C}_j\phi)$
$\mathbf{M}_1' = [A_{ij}']\,i = j,\ A_{ii}' = (C_{Ri}\epsilon j\omega + aS_i^2A/n^2F\phi)(R_o^2/D_iC_{Ri})$
$i \neq j,\ A_{ij}' = (S_iS_jAR_o^2C_{Rj}/n^2F\bar{C}_j\phi)$
$\mathbf{M}_2 = [B_i],\ B_i = S_iAa\Delta\psi_o/nFD_iC_{Ri}$
$\mathbf{M}_2' = [B_i'],\ B_i' = S_iAa\Delta\psi_o/nFD_iC_{Ri}$
$M_1 = (C_{Ri}\epsilon j\omega + aS_1^2A/n^2F\phi)(b^2/D_iC_{R1})$
$M_1' = (C_{Ri}\epsilon j\omega + aS_1^2A/n^2F\phi)(R_o^2/D_iC_{R1})$
$M_2 = -aS_1Ab^2\Delta\psi_o/nFD_1C_{R1}$
$M_2' = aS_1AR_o^2\Delta\psi_o/nFD_1C_{R1}$
$M_3 = -(M_2\Delta\psi_o/M_1)$
$M_3' = (M_2'\Delta\psi_o/M_1')$
n = number of electrons transferred
P = pressure, atm
$Q = (b^2a/\bar{\kappa}\Delta\psi_o)(-A - C_d\omega j)(-\Delta\psi_o + M_3/n\phi + \alpha\sinh\sqrt{M_1}/n\sqrt{M_1}\phi)$
$Q' = (aR_o^2/\bar{\kappa}\Delta\psi_0)(-A - C_d\omega j)(-\Delta\psi_o + M_3'/n\phi + 2\alpha' I_1\sqrt{M_1'}/n\sqrt{M_1'}\phi)$
R_s = external ohmic resistance, ohm
r = radial distance in cylindrical agglomerate, cm
R_o = radius of cylindrical agglomerate, cm
Re = real part of impedance
R = universal gas constant
R_i = reacting species i
S_i = stochiometric coefficient of species i
T = temperature, K
v = voltage, V
$w = \bar{\kappa}Aa$
x = distance in planar agglomerate, cm
$\bar{x} = (x/b)$
z = distance in axial direction, cm
Z = impedance, ohm
$\mathbf{0}$ = zero vector

Greek letters

$\alpha = -M_3/\cosh\sqrt{M_1}$
$\alpha' = -M_3'/\cosh\sqrt{M_1'}$
α_a = anodic transfer coefficient
α_c = cathodic transfer coefficient
$\beta = 1/[\cosh\sqrt{Q} + B\sqrt{Q}\sinh\sqrt{Q}]$
$\beta' = 1/[\cosh\sqrt{Q} + B\sqrt{Q'}\sinh\sqrt{Q'}]$
γ_i = reaction order of species i
Δ = AC part of a signal
$\bar{\kappa}$ = effective ionic conductivity, mho/cm
ω = angular frequency
ϵ = porosity of agglomerate
ϵ' = macroporosity, pore fraction outside agglomerate
$\xi = r/R_o$
$\zeta = z/L$
ψ = electrolyte potential, V
$\Delta\psi_o$ = applied AC perturbation, V
$\phi = F/RT$
$\Psi = \psi/\Delta\psi_o$
η_s = activation polarization, V

Superscripts

$\sim$ = AC part
$-$ = average

Literature Cited

Appleby, A. J., and S. B. Nicholson, "Reduction of Oxygen in Alkali Carbonate Melts," *J. Electroanal. Chem.*, **83,** 309 (1977).

———, "Reduction of Oxygen on Silver Electrodes in Ternary Alkali Carbonate Eutectic Melt," *J. Electrochem. Soc.*, **127,** 759 (1980a).

———, "Reduction of Oxygen in Lithium-Potassium Carbonate Melt," *J. Electroanal. Chem.*, **112,** 71 (1980b).

Argano, E. S., and J. Levitan, "A Dual Reference Electrode System for Molten Carbonate Cells and Immobilized Electrolyte," *J. Electrochem. Soc.*, **116,** 153 (1969).

Armstrong, R. D., K. Edmondson, and J. A. Lee, "The Impedance of Sintered Plate Cadmium Electrode in Alkaline Solution," *J. Electroanal. Chem.*, **63,** 287 (1975).

Bard, A. J., and L. R. Faulkner, *Electrochemical Methods: Fundamentals and Applications*, Wiley, New York (1980).

Broers, G. H. J., and M. Schenke, in *Hydrocarbon Fuel Cell Technology*, B. S. Baker, ed., Academic Press, New York, 225 (1965).

Cachet, C., and R. Wiart, "The Pore Texture of Zinc Electrodes Characterized by Impedance Measurements," *Electrochimica Acta*, **29**, 145 (1984).

Candy, J. P., P. Fouilloux, M. Keddam, and H. Takenouti, "The Characterization of Porous Electrodes by Impedance Measurements," *Electrochim. Acta*, **26**, 1029 (1981).

———, "The Pore Texture of Raney Nickel Determined by Impedance Measurements," *Electrochim. Acta*, **27**, 1585 (1982).

Delnick, F. M., S. C. Jaeger, and S. C. Levy, "An Impedance Study of Porous Carbon Collectors for Li/SO_2 Primary Cells," Paper 34d, Am. Inst. Chem. Eng. meeting, L.A., CA (Nov., 1983).

Giner, J., and C. Hunter, "The Mechanism of Operation of the Teflon-Bonded Gas Diffusion Electrode: A Mathematical Model," *J. Electrochem. Soc.*, **116**, 1124 (1969).

Keiser, H., K. D. Deccu, and M. A. Gutjahr, "Abschatzung der Porenstruktur Poroser Elektroden aus Impedanzmessunchen (Estimation of Pore Structure of Porous Electrodes from Impedance Measurement)," *Electrochim. Acta*, **21**, 539 (1976).

Kunz, H. R., L. J. Bregoli, and S. Y. Szymanski, "A Homogenous/Agglomerate Model for Molten Carbonate Cathodes," *J. Electrochem. Soc.*, **131**, 2815 (1984).

de Levie, R., "Electrochemical Responses of Porous and Rough Electrodes," *Adv. Electrochem. Electrochem. Eng.*, **6**, 329 (1967).

Mund, K., M. Edeling, and G. Richter, "Impedance Measurements with Porous Electrodes for Electrochemical Energy Conversion and Storage," Abstract 274, *Extended Abstract 82-2*, Electrochem. Soc. Pennington, NJ (1982).

Selman, J. R., and L. G. Marianowski, "Fuel Cells," *Molten Salt Technology*, D. G. Lovering, ed., Plenum, New York (1982).

Selman, J. R., and H. C. Maru, "Physical Chemistry and Electrochemistry of Alkali Carbonate Melts," *Advances in Molten Salt Chemistry, 4*, G. Mamantov, J. Braunstein, eds., Plenum, New York, 159 (1983).

Smith, S. W., W. M. Vogel, and S. Kapelner, "Solubility of Oxygen in Fused Lithium Carbonate–Potassium Carbonate," *J. Electrochem. Soc.*, **129**, 1668 (1982).

Smyrl, W. H., "Digital Impedance for Faradaic Analysis," *J. Electrochem. Soc.*, **132**, 1551 (1984).

Uchida, I., and T. Nishina, "Potential-pO^{-2} Diagrams of Oxygen Electrode in Molten Carbonate," Abstract 195, *Extended Abstracts 87-2*, Electrochem. Soc., Pennington, NJ (1987).

Uchida, I., T. Nishina, Y. Mugikura, and K. Itaya, "Gas Electrode Reactions in Molten Carbonate Media. I: Exchange Current Density of Oxygen Reduction in (Li + K)CO_3 Eutectic at 650°C. II: Oxygen Reduction Kinetics on Conductive Oxide Electrodes in (Li + K)CO_3 Eutectic at 650°C," *J. Electroanal. Chem.*, **206**, 229 (1986).

Vogel, W. M., S. W. Smith, and L. J. Bregoli, "Studies of the Reduction of Oxygen on Gold in Molten Lithium Carbonate–Potassium Carbonate at 650°C," *J. Electrochem. Soc.*, **130**, 574 (1983).

Wilemski, G., "Simple Porous Electrode Models for Molten Carbonate Fuel Cell," *J. Electrochem. Soc.*, **130**, 117 (1983).

Winnick, J., and P. N. Ross, Jr., "The Kinetics for the O_2/CO_2 Reduction in Molten Carbonate: Reaction Orders for Oxygen and CO_2 on Porous NiO," *J. Electrochem. Soc.*, **128**, 991 (1981).

Yuh, C. Y., "Potential Relaxation and AC Impedance of Porous Electrodes," Ph.D. Thesis, Ill. Inst. Technol., Chicago (Dec., 1985).

Yuh, C. Y., and J. R. Selman, "Polarization of the Molten Carbonate Fuel Cell Anode and Cathode," *J. Electrochem. Soc.*, **131**, 2062 (1984).

———, "The Polarization of Molten Carbonate Fuel Cell Electrodes. I: Analysis of Steady-State Polarization Data," submitted *J. Electrochem. Soc.* (1988).

Manuscript received May 15, 1987, and revision received July 21, 1988.